Ballistic transport, chiral anomaly, and emergence of the neutral electron-hole plasma in graphene

H. C. Kao,[1] M. Lewkowicz,[2] and B. Rosenstein[2,3,*]
[1]*Physics Department, National Taiwan Normal University, Taipei, Taiwan, Republic of China*
[2]*Applied Physics Department, Ariel University Center of Samaria, Ariel 40700, Israel*
[3]*Electrophysics Department, National Chiao Tung University, Hsinchu 30050, Taiwan, Republic of China*
(Received 7 April 2010; published 7 July 2010)

The process of coherent creation of particle-hole excitations by an electric field in graphene is quantitatively described using a dynamic "first-quantized" approach. We calculate the evolution of current density, number of pairs, and energy in ballistic regime using the tight-binding model. The series in electric field strength E up to third order in both dc and ac are calculated. We show how the physics far from the two Dirac points enters various physical quantities in linear response and how it is related to the chiral anomaly. The third harmonic generation and the imaginary part of conductivity are obtained. It is shown that at certain time scale $t_{nl} \propto E^{-1/2}$ the physical behavior dramatically changes and the perturbation theory breaks down. Beyond the linear-response physics is explored using an exact solution of the first-quantized equations. While for small electric fields the I-V curve is linear characterized by the universal minimal resistivity $\sigma = \pi/2(e^2/h)$, at $t > t_{nl}$ the conductivity grows fast. The copious pair creation (with rate $E^{3/2}$), analogous to Schwinger's electron-positron pair creation from vacuum in QED, leads to creation of the electron-hole plasma at ballistic times of order t_{nl}. This process is terminated by a relaxational recombination.

DOI: 10.1103/PhysRevB.82.035406 PACS number(s): 73.61.−r, 11.10.Kk, 73.20.Mf, 73.23.Ad

I. INTRODUCTION

It has been demonstrated recently that a graphene sheet, especially one suspended on leads, is one of the purest electronic systems. It became increasingly evident that electronic mobility in graphene is extremely large exceeding that in best semiconductor two-dimensional (2D) systems.[1] The scattering of charge carriers in suspended graphene samples of submicron length is so negligible that the transport is ballistic.[2,3] The ballistic flight time can be estimated as $t_{bal} = L/v_g$, where v_g is the graphene velocity characterizing the "relativistic" spectrum of graphene near Dirac points and L is the length of the sample. During the ballistic flight conductivity calculated neglecting interactions with phonons, ripplons, disorder, and between electrons, etc., are consistent with experiments at least near the Dirac point at which no carriers are present.[4]

In a simplified model of a single graphene sheet (neglecting scattering processes and electron interactions) the chemical potential is located right between the valence and conductance bands and the Fermi "surface" consists of two Dirac points of the Brillouin zone.[5] A lot of effort has been devoted theoretically to the question of dc and ac transport in pure graphene due to the surprising fact that the conductivity is finite without any dissipation process present. A widely accepted "standard" value of the "minimal dc conductivity" at zero temperature,

$$\sigma_1 = \frac{4}{\pi}\frac{e^2}{h} \tag{1}$$

was calculated using a simplified Dirac model[5–10] by a variety of methods. Direct application of the Kubo formula at zero frequency, disorder strength, temperature, and chemical potential[6,8] utilizes certain "regularizations" such as the $i\eta$ regulator which is interpreted as an "infinitesimal disorder." The regulator is removed at the end of the calculation. A more customary application of the Kubo formula starts with finite frequency. As noted by Ziegler and co-workers[8] the order of limits makes a difference and several other values different from σ_1 were provided for the *same* system. The standard value σ_1 is obtained using a rather unorthodox procedure when the dc limit $\omega \to 0$ is made *before* the zero disorder strength limit $\eta \to 0$ is taken. If the order of limits is reversed, one obtains[8]

$$\sigma_2 = \frac{\pi}{2}\frac{e^2}{h}. \tag{2}$$

When the limit is taken holding $\omega = \eta$ one can even obtain a value of $\sigma_3 = \pi\frac{e^2}{h}$,[8] thus solving the "missing π" problem (the same value was obtained very recently using yet another regularization in Ref. 11). Indeed, at least early experiments on graphene sheets on Si substrates provided values roughly three times larger than σ_1.[12] Recent experiments on suspended graphene[2] demonstrated that the dc conductivity is lower, $1.7\sigma_1$, as temperature is reduced to 4 K. Hence while σ_3 seems to be inconsistent with experiment, one still faces the question of what is the proper theoretical value. Since the conductivity of clean graphene in the infinite sample is a well-defined physical quantity, there cannot be any ambiguity as to its theoretical value. Another theoretical approach to the problem was the use of Landauer formalism to the graphene sheet conductance. The conductivity appears as a limiting value of infinite width W in this approach[9,10] and one obtains σ_1. Also resumming the series in disorder by a self-consistent Born approximation gives σ_1 (Ref. 7) while other resummations can lead to a different result.[13]

In contrast to the controversy with respect to the dc conductivity, both the experimental and the theoretical situation for the ac conductivity in the high-frequency limit is quite

different. The theoretically predicted value in the Dirac model is σ_2 independent of frequency under condition $\omega \gg T/\hbar$.[7,14] The Dirac model becomes inapplicable when ω is of order of $\gamma/\hbar \approx 4\times 10^{15}$ Hz or larger, where γ is the hopping energy of graphene. It was shown theoretically using the tight-binding model and experimentally in Ref. 15 that the optical conductivity at frequencies higher or of order $\gamma/\hbar$ becomes slightly larger than σ_2. Moreover, in light transmittance measurements at frequencies down to 2.5×10^{15} Hz it was found equal to σ_2 within 4%. The tight-binding model *does not contain any other time* scales capable of changing the limiting value of the ac conductivity all the way to $\omega \to 0$. Therefore one would expect that the dc conductivity is σ_2 rather than σ_1.

As is shown in the present paper, using the dynamical approach (a brief account of some results was published in Refs. 4 and 6), this is indeed the case. The basic physical effect of the electric field is a coherent creation of electron-hole pairs, mostly but not exclusively, near the two Dirac points. To effectively describe this process we develop a dynamical approach to charge transport in clean graphene using the "first-quantized" approach to pair-creation physics similar to that developed in relativistic physics[17] to describe electron-positron pairs creation. To better visualize the phenomenon of resistivity without dissipation directly at zero temperature, doping, frequency, and disorder we describe an experimental situation as closely as possible by calculating directly the time evolution of the electric current after switching on an electric field. In this way the use of a rather formal Kubo or Landauer formalism is avoided and as a result *no regularizations are needed*. Although we consider an infinite sample, the dynamical approach allows us to obtain qualitative results for finite samples by introducing time cutoffs such as ballistic flight time. Various other factors determining transport can be conveniently characterized by time scales such as the relaxation time for scattering of phonons or impurities.

We show in detail that some aspects the linear-response physics are not dominated by the two Dirac points of the Brillouin zone at which the spectrum is gapless. For example, large contributions [infinite, when the size of the Brillouin zone $2\pi/a$ (a=3 Å is the lattice spacing), is being considered infinite] to the conductivity from the vicinity of the Dirac points are canceled by contributions from the region between them. This phenomenon is related to the chiral anomaly in field theory.[18] We analyze the use of massless Dirac (Weyl) model approximation to the tight-binding model and propose an effective chirally invariant regularization for it.

In addition to the analysis of the linear response, we determin the range of applicability of the linear-response approximation by both calculation of higher orders in (dc and ac) electric field and solving the model exactly in the nonlinear electromagnetic response regime. Only the zero chemical-potential case (no net charge) is considered. In this respect the work is complimentary to an earlier study by Mikhailov[19] in which ballistic nonlinear electromagnetic response to an ac field was calculated at finite chemical potential using the Boltzmann equation within a semiclassical approach and major effects we study were omitted. We first obtain perturbative corrections up to the third order in the electric field E. At this order qualitatively distinct phenomena such as the third harmonic generation and the imaginary part of conductivity appear. The calculation of the corrections allows us to estimate the time scale at which perturbation theory breaks down. At this scale, $t_{nl} \propto E^{-1/2}$, the physical behavior is expected to change qualitatively. Therefore one has to resort to nonperturbative methods. Certain aspects of nonlinear ac response at zero chemical potential were also studied recently by Mishchenko.[20] In his work disorder (taken into account phenomenologically) dominates the purely ballistic effects by cutting off the ballistic times at relaxation-time scale before t_{nl} is reached.

Physics of the simplest tight-binding model beyond the linear response is explored via an exact solution of the first-quantized equations. It is a peculiar property of the tight-binding model in the dynamical approach, that the exact solution of the equations for arbitrary momentum k_y can be reduced to that for k_y=0; the constant electric field being in the y direction. Moreover, the remaining equations, using Floquet theory, can then be reduced to a recursion relation. We use this property to effectively calculate the long ballistic flight evolution of various physical quantities such as the current density and the number of created pairs. While for small ballistic times, $t < t_{nl}$, the conductivity settles at σ_2, at $t > t_{nl}$ the current grows linearly. This increase can be explained using Schwinger's electron-positron pair-creation mechanism.[21] The pair creation is a two-dimensional version of that in QED with the creation rate proportional to $E^{3/2}$.[22] This, in absence of relaxation channels (for times below $t_{bal}=L/v_g$), leads to the creation of a neutral electron-hole plasma at ballistic times of order t_{nl}. This process cannot continue forever and is terminated by a relaxational recombination. The applicability of Schwinger's formula for the electron-hole pairs creation rate was debated over a long time and we set the limitation on the applicability of this exact formula to graphene.

The rest of the paper is organized as follows. The tight-binding model and the dynamical approach are described in Sec. II. The perturbation theory in electric field is described in Sec. III. The minimal conductivity is obtained and the role of states beyond the neighborhoods of the Dirac points (and their relation to "axial anomaly" and the Nielsen-Ninomya theorem) is clarified. The dynamical linear-response approach to the ac field is considered. In Sec. IV perturbative corrections beyond linear response (up to third order in E) are calculated. The third harmonic and inductive contributions to conductivity are discussed. The exact solution for arbitrary field is constructed using the Floquet theory in Sec. V. It is used in Sec. VI to discuss the pair-creation rate, conductivity, and speculate about the electron-hole plasma. Finally Sec. VII contains discussion and conclusions.

II. MODEL AND THE DYNAMIC APPROACH TO ITS PHYSICAL PROPERTIES

A. Tight-binding model in an electric field

Electrons in graphene are described sufficiently accurately for our purposes by the 2D tight-binding model of nearest-

neighbor interactions.[5] The Hamiltonian in $\mathbf{k}$ space is

$$\hat{H} = \sum_{\mathbf{k}} (c_{\mathbf{k}}^{A\dagger} \quad c_{\mathbf{k}}^{B\dagger}) H_{\mathbf{k}} \begin{pmatrix} c_{\mathbf{k}}^{A} \\ c_{\mathbf{k}}^{B} \end{pmatrix}, \tag{3}$$

where

$$H_{\mathbf{k}} = \begin{pmatrix} 0 & h_{\mathbf{k}} \\ h_{\mathbf{k}}^{*} & 0 \end{pmatrix}, \quad h_{\mathbf{k}} = -\gamma \sum_{\alpha} e^{i\mathbf{k}\cdot\boldsymbol{\delta}_{\alpha}} \tag{4}$$

with $\gamma \simeq 2.7$ eV being the hopping energy; $\boldsymbol{\delta}_1 = \frac{a}{3}(0, \sqrt{3})$ and $\boldsymbol{\delta}_{2,3} = \frac{a}{3}(\pm\frac{3}{2}, -\frac{\sqrt{3}}{2})$ are the locations of nearest neighbors separated by distance $a \simeq 3$ Å; and the pseudospin index A, B denotes two triangular sublattices. In most parts of the paper we keep the function $h_{\mathbf{k}}$ arbitrary. Let us first consider the system in a constant and homogeneous electric field along the y direction switched on at $t=0$. It is described by the minimal substitution,

$$\mathbf{p} = \hbar\mathbf{k} + \frac{e}{c}\mathbf{A}, \tag{5}$$

with vector potential $\mathbf{A} = (0, -cEt)$ for $t > 0$ ($e > 0$). Later it is generalized to more general fields including the ac field.

B. Dynamical first-quantized approach

Since the crucial physical effect of the field is mainly a coherent creation of electron-hole pairs (though not always near the Dirac points, see below), a convenient formalism to describe the pair creation is the first-quantized formulation described in detail in Ref. 17. The spectrum before the electric field is switched on is divided into positive- and negative-energy parts describing the valence and conduction bands

$$H_{\mathbf{k}}(E=0)u_{\mathbf{k}} = -\varepsilon_{\mathbf{k}} u_{\mathbf{k}}, \quad u_{\mathbf{k}} = \begin{pmatrix} 1 \\ -h_{\mathbf{k}}^{*}/\varepsilon_{\mathbf{k}} \end{pmatrix}, \tag{6}$$

$$H_{\mathbf{k}}(E=0)v_{\mathbf{k}} = \varepsilon_{\mathbf{k}} v_{\mathbf{k}}, \quad v_{\mathbf{k}} = \begin{pmatrix} 1 \\ h_{\mathbf{k}}^{*}/\varepsilon_{\mathbf{k}} \end{pmatrix}, \tag{7}$$

where $\varepsilon_{\mathbf{k}} = |h_{\mathbf{k}}|$. A second-quantized state is uniquely characterized by the first-quantized amplitude,

$$\psi_{\mathbf{k}}(t) = \begin{pmatrix} \psi_{\mathbf{k}}^{1}(t) \\ \psi_{\mathbf{k}}^{2}(t) \end{pmatrix}, \tag{8}$$

which is a "spinor" in the sublattice space. It obeys the matrix Schroedinger equation in sublattice space

$$i\hbar\partial_t \psi_{\mathbf{k}} = H_{\mathbf{p}}\psi_{\mathbf{k}}, \tag{9}$$

where $\mathbf{p}$ is defined in Eq. (5). The initial condition corresponding to a second-quantized state at $T=0$ in which all the negative-energy states are occupied and all the positive-energy states are empty is

$$\psi_{\mathbf{k}}(t=0) = u_{\mathbf{k}}. \tag{10}$$

A physical quantity is usually conveniently written in terms of ψ. We will be interested mostly in the current density (multiplied by factor 2 due to spin)

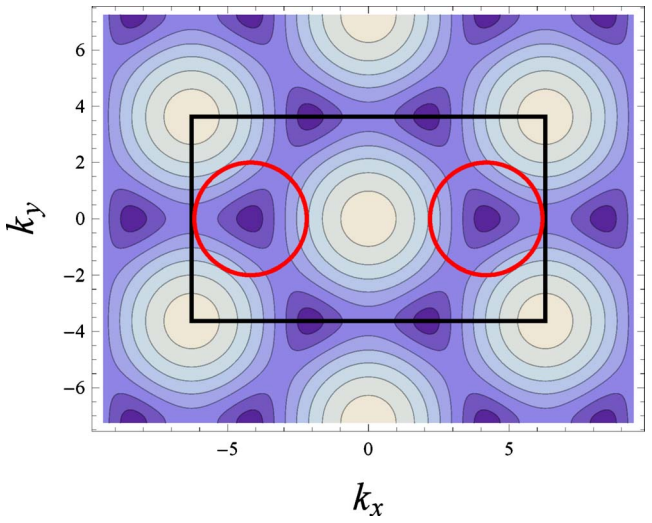

FIG. 1. (Color online) Constant energy map of the honeycomb-lattice Brillouin zone. The rectangle outlines two Brillouin zones, the area of integration in Eqs. (11) and (31). The circles show the vicinity of the two Dirac points with radius Λ for the integration in Eq. (34).

$$J_y(t) = -2e \sum_{\mathbf{k}\in BZ} \psi_{\mathbf{k}}^{\dagger}(t) \frac{\partial H_{\mathbf{p}}}{\partial p_y} \psi_{\mathbf{k}}(t), \tag{11}$$

as well as the energy and the density of the electron-hole pairs. The summation is over the honeycomb-lattice Brillouin zone, see Fig. 1, in which two Brillouin zones are outlined. The energy of the electrons is changing due to the applied electric field (with no dissipation in the ballistic regime, see, however, Sec. VII) and is given by

$$U(t) = 2\sum_{\mathbf{k}} \psi_{\mathbf{k}}^{\dagger}(t) H_{\mathbf{p}} \psi_{\mathbf{k}}(t). \tag{12}$$

The amplitude of lifting an electron into the conduction band (defined for the Hamiltonian without the electric field) is $\langle \psi(t) | v_{\mathbf{k}} \rangle$, where the scalar product is defined by $\langle \psi | \phi \rangle = \psi_1^{*}\phi_1 + \psi_2^{*}\phi_2$, and consequently the density of pairs reads

$$N_0(t) = 2\sum_{\mathbf{k}} |\langle \psi(t) | v_{\mathbf{k}} \rangle|^2 = 2\sum_{\mathbf{k}} \left| \psi_1^{*} + \frac{h_{\mathbf{k}}^{*}}{\varepsilon_{\mathbf{k}}} \psi_2^{*} \right|^2. \tag{13}$$

Since the Hamiltonian depends on time via the vector potential that shifts the momentum $\mathbf{p}$, a more useful definition of the density of pairs taking into account the shift of the momentum will be given in Sec. III.

C. Units and conventions

The units of energy, time, and distance are defined by the microscopic values γ, $t_\gamma \equiv \hbar/\gamma (\simeq 2.5 \times 10^{-16}$ s) and a, correspondingly. The unit of the electric field will be $E_0 \equiv \frac{\gamma}{ea} \simeq 10^{10}$ V/m so that the dimensionless electric field is $\mathcal{E} = E/E_0$ and the unit of conductivity will be $e^2/\hbar$. Effectively one can set $\gamma = \hbar = a = e = 1$. In these units the first-quantized equation reads

$$i\partial_t \psi_1 = h_{\mathbf{p}}\psi_2,$$

$$i\partial_t \psi_2 = h_{\mathbf{p}}^* \psi_1, \tag{14}$$

where the tight-binding Hamiltonian matrix element $h_{\mathbf{p}}$ takes the form

$$h_{\mathbf{p}} = -\exp\left(i\frac{p_y}{\sqrt{3}}\right) - b\exp\left(-i\frac{p_y}{2\sqrt{3}}\right), \tag{15}$$

where $b=2\cos(\frac{p_x}{2})$, and $p_y=k_y+A_y$, $A_y=-\mathcal{E}t$ for the dc field. We will use extensively its expansion in powers of A_y

$$\frac{dh_{\mathbf{p}}}{dA_y} \equiv h'_{\mathbf{p}} = -\frac{i}{\sqrt{3}}\exp\left(i\frac{p_y}{\sqrt{3}}\right) + \frac{ib}{2\sqrt{3}}\exp\left(-i\frac{p_y}{2\sqrt{3}}\right),$$

$$\frac{d^2h_{\mathbf{p}}}{dA_y^2} \equiv h''_{\mathbf{p}} = \frac{1}{3}\exp\left(i\frac{p_y}{\sqrt{3}}\right) + \frac{b}{12}\exp\left(-i\frac{p_y}{2\sqrt{3}}\right). \tag{16}$$

For example, the off-diagonal matrix element for the $\mathbf{p}$ component of the current J_y is $-h'_{\mathbf{p}}$, so that the current density, using the first-quantized approach, is

$$J_y = -2\sum_{\mathbf{k}} \psi_{\mathbf{p}}^\dagger \begin{pmatrix} 0 & h'_{\mathbf{p}} \\ h_{\mathbf{p}}^{*\prime} & 0 \end{pmatrix} \psi_{\mathbf{p}}. \tag{17}$$

The next two sections deal with the perturbative treatment of the electric field and later (after having shown that it fails at certain time scale) we will switch to a nonperturbative method.

III. LINEAR RESPONSE, THE PSEUDODIFFUSIVE BEHAVIOR, AND THE PARITY ANOMALY

A. Expansion in electric field

Expanding in the dimensionless electric field strength (assumed for simplicity homogeneous and constant after switching on the field at $t=0$), $\psi_{\mathbf{k}}=e^{i\varepsilon_{\mathbf{k}}t}(u_{\mathbf{k}}+\mathcal{E}\xi_{\mathbf{k}}+\cdots)$, one obtains for the first correction the following equation:

$$i\partial_t \xi_{\mathbf{k}} = \begin{pmatrix} \varepsilon_{\mathbf{k}} & h_{\mathbf{k}} \\ h_{\mathbf{k}}^* & \varepsilon_{\mathbf{k}} \end{pmatrix} \xi_{\mathbf{k}} - t\begin{pmatrix} 0 & h'_{\mathbf{k}} \\ h_{\mathbf{k}}^{*\prime} & 0 \end{pmatrix} u_{\mathbf{k}}. \tag{18}$$

Writing the correction as $\xi_{\mathbf{k}}=\alpha_{\mathbf{k}}u_{\mathbf{k}}+\beta_{\mathbf{k}}v_{\mathbf{k}}$, it takes the form

$$i\partial_t \alpha_{\mathbf{k}} = t\varepsilon'_{\mathbf{k}},$$

$$i\partial_t \beta_{\mathbf{k}} = 2\varepsilon_{\mathbf{k}}\beta_{\mathbf{k}} - t\varepsilon_{\mathbf{k}}\bar{I_{\mathbf{k}}} \tag{19}$$

with initial conditions $\alpha_{\mathbf{k}}(t=0)=1$ and $\beta_{\mathbf{k}}(t=0)=0$. We use the abbreviations

$$\varepsilon'_{\mathbf{k}} \equiv \frac{\partial \varepsilon_{\mathbf{k}}}{\partial k_y} \tag{20}$$

and

$$\bar{I_{\mathbf{k}}} \equiv \frac{h_{\mathbf{k}}^* h'_{\mathbf{k}} - h_{\mathbf{k}} h_{\mathbf{k}}^{*\prime}}{2\varepsilon_{\mathbf{k}}^2}. \tag{21}$$

The coefficient $\beta_{\mathbf{k}}$ denotes the amplitude of accumulation of electrons in the conduction band whereas $\alpha_{\mathbf{k}}$ denotes the amplitude of remaining in the valence band. Solving the equations one obtains

$$\alpha_{\mathbf{k}} = -\frac{i}{2}t^2\varepsilon'_{\mathbf{k}}, \quad \beta_{\mathbf{k}} = \frac{i\bar{I_{\mathbf{k}}}}{4\varepsilon_{\mathbf{k}}}(1 - e^{-2i\varepsilon_{\mathbf{k}}t} - 2i\varepsilon_{\mathbf{k}}t). \tag{22}$$

The expansion for the current, Eq. (11), in the electric field up to the first order contains the following momentum $\mathbf{k}$ contributions, $J_y=\Sigma_{\mathbf{k}} j_{\mathbf{k}}$:

$$j_{\mathbf{k}} = j_{\mathbf{k}}^0 + j_{\mathbf{k}}^p + j_{\mathbf{k}}^d. \tag{23}$$

The zero-order contribution is

$$j_{\mathbf{k}}^0 = -u_{\mathbf{k}}^\dagger \begin{pmatrix} 0 & h'_{\mathbf{k}} \\ h_{\mathbf{k}}^{*\prime} & 0 \end{pmatrix} u_{\mathbf{k}} = 2\varepsilon_{\mathbf{k}} I_{\mathbf{k}}^+, \tag{24}$$

where

$$I_{\mathbf{k}}^+ = \frac{h_{\mathbf{k}} h_{\mathbf{k}}^{*\prime} + h_{\mathbf{k}}^* h'_{\mathbf{k}}}{2\varepsilon_{\mathbf{k}}^2}. \tag{25}$$

The correction gives the "paramagnetic" and "diamagnetic" contributions to the current densities

$$j_{\mathbf{k}}^p = -2\mathcal{E}u_{\mathbf{k}}^\dagger \begin{pmatrix} 0 & h'_{\mathbf{k}} \\ h_{\mathbf{k}}^{*\prime} & 0 \end{pmatrix} \xi_{\mathbf{k}} + \text{c.c.} = 2\mathcal{E}(\alpha_{\mathbf{k}} - \alpha_{\mathbf{k}}^*)\varepsilon_{\mathbf{k}}\bar{I_{\mathbf{k}}}$$

$$= \mathcal{E}(\bar{I_{\mathbf{k}}})^2[2\varepsilon_{\mathbf{k}}t - \sin(2\varepsilon_{\mathbf{k}}t)], \tag{26}$$

$$j_{\mathbf{k}}^d = \mathcal{E}tu_{\mathbf{k}}^\dagger \begin{pmatrix} 0 & h''_{\mathbf{k}} \\ h_{\mathbf{k}}^{*\prime\prime} & 0 \end{pmatrix} u_{\mathbf{k}} = -2\mathcal{E}t\varepsilon_{\mathbf{k}} I_{\mathbf{k}}^+. \tag{27}$$

Both corrections for a specific momentum $\mathbf{k}$ diverge at large ballistic times as t, however, one still has to integrate over the valence-band momenta.

B. Integration over momenta and physical interpretation of the "quasi-Ohmic" behavior

To first order in electric field the current density is

$$J_y = J_0 + \sigma\mathcal{E}, \tag{28}$$

where the zero-order contribution can be written as a derivative with respect to k_y of a periodic function

$$J_0 = -2\sum_{\mathbf{k}} j_{\mathbf{k}}^0 = 4\sum_{\mathbf{k}} \varepsilon'_{\mathbf{k}}. \tag{29}$$

It vanishes upon integration, in accordance with the Bloch theorem since the Brillouin zone can be chosen in such a way that it exhibits periodicity in the field (y) direction. For example, we can integrate over the rectangular area shown in Fig. 1 containing two Brillouin zones

$$\sum_{BZ} = \frac{1}{2}\frac{1}{(2\pi)^2}\int_{-2\pi}^{2\pi} dk_x \int_{-2\pi/3^{1/2}}^{2\pi/3^{1/2}} dk_y. \tag{30}$$

It should be noted that $\int_{-2\pi/3^{1/2}}^{2\pi/3^{1/2}} \varepsilon'_{\mathbf{k}} dk_y = \varepsilon_{k_x,2\pi/3^{1/2}} - \varepsilon_{k_x,-2\pi/3^{1/2}} = 0$ at every k_x, and due to the continuity of $\varepsilon_{\mathbf{k}}$ even at the Dirac points. Therefore one is left with the linear response.

The conductivity can be divided into an apparently linearly divergent part and a finite part, $\sigma(t)=\sigma_{BZ}(t)+\sigma_{DP}(t)$. As will be explained shortly, the contributions to the first

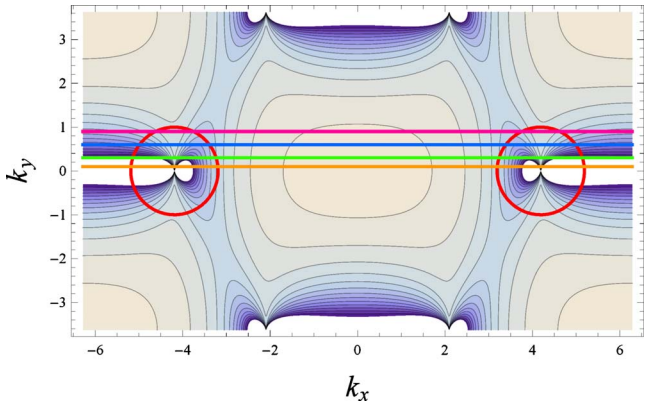

FIG. 2. (Color online) The integrand of σ_{BZ} Eq. (31) is plotted within the integration area shown in Fig. 1. The integrand is negative along the line connecting two Dirac points along the field direction and positive elsewhere.

term at large t stem mostly from the immediate neighborhoods of the two Dirac points while contributions to the second come from whole Brillouin zone. The part diverging linearly with time can be written (after some algebra) as a full derivative with respect to k_y

$$\sigma_{BZ}(t) = t\sum_{\mathbf{k}} \frac{(h_{\mathbf{k}}h_{\mathbf{k}}^{*\prime} - h_{\mathbf{k}}^{*}h_{\mathbf{k}}^{\prime})^2 - 2\varepsilon_{\mathbf{k}}^2(h_{\mathbf{k}}h_{\mathbf{k}}^{*\prime\prime} + h_{\mathbf{k}}^{*}h_{\mathbf{k}}^{\prime\prime})}{\varepsilon_{\mathbf{k}}^3} = -4t\sum_{\mathbf{k}} \varepsilon_{\mathbf{k}}^{\prime\prime}. \tag{31}$$

This too vanishes upon integration over the Brillouin zone since it is again an integral of a derivative of a periodic function, albeit this cancellation is nontrivial. In Fig. 2 the integrand of Eq. (31) is plotted within the integration area specified above, Eq. (30). The integrand is negative along the line connecting two Dirac points along the field direction, for example,

$$\mathbf{K}_L = 2\pi\left(\frac{1}{3}, \frac{1}{\sqrt{3}}\right), \quad \mathbf{K}_R = 2\pi\left(-\frac{1}{3}, \frac{1}{\sqrt{3}}\right) \tag{32}$$

(recall that $a=1$ in our units), and positive elsewhere. In Fig. 3 several cross sections for various k_x values are shown. One

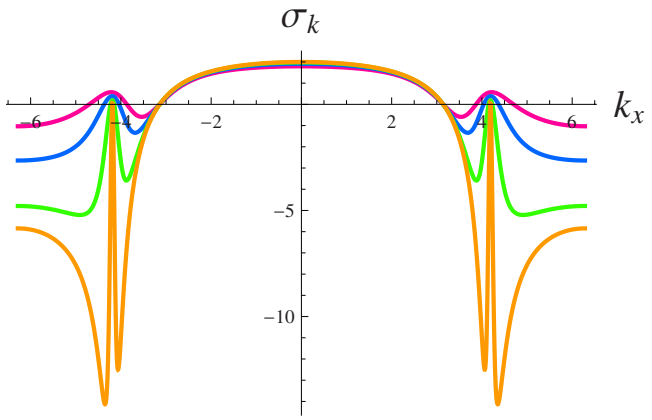

FIG. 3. (Color online) Several cross sections of the integrand of σ_{BZ} Eq. (31) are shown for various k_x values as indicated in Fig. 2.

observes, that as k_x approaches $2\pi/3$ the integrand goes to $-\infty$ at $k_y=2\pi/\sqrt{3}$, corresponding to Dirac point $\mathbf{K}_L$. Consequently for all $k_x \neq 2\pi/3$, the integrand is a regular function, and thus the integral over k_y vanishes. At $k_x=2\pi/3$ the integral over k_y is finite, yet does not influence the two-dimensional integral.

The remaining part

$$\sigma_{DP}(t) = -2\sum_{\mathbf{k}} (I_{\mathbf{k}}^{-})^2 \sin(2\varepsilon_{\mathbf{k}}t) \tag{33}$$

gives a finite result. Unlike the divergent part of the conductivity, the integral for $t \gg 1$ (in units of t_γ) is dominated by contributions from the vicinity of the two Dirac points [circles in Fig. 2 of radius $\Lambda \simeq 1$ (in units of $\hbar/a$)]. Indeed the prefactor $(I_{\mathbf{k}}^{-})^2$ is bounded from above by Λ^{-2} and integral over the area outside the circles vanishes at $t \gg 1/\Lambda$. The contribution of a single Dirac point is obtained by integrating to infinity (in polar coordinates centered at the Dirac point),

$$\frac{\sigma_{DP}}{2} = \frac{1}{(2\pi)^2}\int_{\varphi=0}^{2\pi}\int_{q=0}^{\Lambda} \sin(\varphi)^2 \frac{\sin(2v_g q t)}{q} = \frac{1}{4\pi}\int_{q'=0}^{2v_g\Lambda t} \frac{\sin(q')}{q'}. \tag{34}$$

At long time the upper limit can be replaced by infinity which results

$$\sigma_{DP} = \frac{1}{2\pi}\mathrm{Si}(\infty) = \frac{1}{4}. \tag{35}$$

Here one can safely multiply the result by the valley degeneracy 2. Returning to physical units, one obtains $\sigma=\sigma_2$, Eq. (2).

The dependence on time was calculated numerically. After an initial increase on the natural time scale $t_\gamma \equiv \hbar/\gamma$ the conductivity approaches σ_2 via oscillations, see Fig. 1 in Ref. 4. The amplitude of oscillations decays as a power $\frac{\sigma}{\sigma_2} \approx 1 + \frac{\sin(2t)}{2t}$ (for $t \gg t_\gamma$).

A physical picture of this resistivity without dissipation is as follows. The electric field creates electron-hole excitations in the vicinity of the Dirac points in which electrons behave as massless relativistic fermions with the graphene velocity v_g playing the role of the light velocity. For such particles the absolute value of the velocity is v_g and cannot be altered by the electric field and is not related to the wave vector $\mathbf{k}$. On the other hand, the orientation of the velocity is influenced by the applied field. The electric current is $e\mathbf{v}$, thus depending on orientation, so that its projection on the field direction y is increased by the field. An important observation, made, for example, in Ref. 23, is that the electric field while creating charge transport, does not change the overall momentum. As a consequence the effects of impurities do not affect the pair creation in the same way they affect "free" carriers. These two sources of current, namely, creation and reorientation are roughly of the same size in the linear response. As we will see below, the situation changes at ballistic times when the linear response breaks down.

C. Pair-creation rate

In analogy to the linear response in the current, the pair-creation rate per unit area, as defined in Eq. (13), can be calculated and to leading order in $\mathcal{E}$ is

$$\frac{d}{dt}N_0 = -2t\sum_{\mathbf{k}}[I_{\mathbf{k}}\sin(2\varepsilon_{\mathbf{k}}t)]^2\mathcal{E}^2. \tag{36}$$

The result of the numerical integration over the Brillouin zone was given in Fig. 2 of Ref. 16. It is dominated by the two Dirac points and at large times (compared to t_γ) behaves as

$$\frac{d}{dt}N_0 \simeq \frac{2}{\pi}\mathcal{E}^2 t\log(t). \tag{37}$$

It is, however, well known that a dc electric field in QED (even with massive relativistic electrons) renders the vacuum unstable,[17,21] with the "renormalized" number of pairs depending on $\mathcal{E}^{3/2}$. Therefore nonperturbative effects are expected and will be studied below.

The notion of renormalized number of pairs is a consequence of the fact that for unstable systems the Fermi level should be continuously renormalized as a function of time. In the first-quantized formalism this corresponds to a continuous modification of the "initial" state $v_{\mathbf{k}}\to v_{\mathbf{p}}=v_{\mathbf{k}-\mathcal{E}t}$ defining holes. This leads to the following definition of the pair density:[24]

$$N_p(t) = 2\sum_{\mathbf{k}\in BZ}|\langle\psi(t)|v_{\mathbf{p}}\rangle|^2 = 2\sum_{BZ}\left|\psi_1^* + \frac{h_{\mathbf{p}}^*}{\varepsilon_{\mathbf{p}}}\psi_2^*\right|^2. \tag{38}$$

It is used in the framework of the relativistic Dirac model and was recently extensively discussed in Ref. 22 in connection with graphene (using the instanton approximation).

D. ac field

A similar calculation within the dynamic first quantization formalism for the evolution of the current density can be performed for an arbitrary time dependence of the homogeneous electric field. Let us consider an arbitrary time dependence of the y component of the vector potential $A_y=-\mathcal{E}a(t)$, subject to a "switching on" condition, $a(t)=0$, for $t<0$. Fourier transforms are defined by

$$a(t) = \int_\omega e^{-i\omega t}a(\omega), \quad \xi_{\mathbf{k}}(t) = \int_\omega e^{-i\omega t}\xi_{\mathbf{k}}(t), \tag{39}$$

and similarly for the current density and other quantities. The next to leading order in $\mathcal{E}$ first-quantized tight-binding equations are

$$-a(\omega)\begin{pmatrix}0 & h_{\mathbf{k}}'\\ h_{\mathbf{k}}^{*\prime} & 0\end{pmatrix}u_{\mathbf{k}} + \begin{pmatrix}\varepsilon_{\mathbf{k}}-\omega & h_{\mathbf{k}}\\ h_{\mathbf{k}}^* & \varepsilon_{\mathbf{k}}-\omega\end{pmatrix}\xi_{\mathbf{k}}(\omega) = 0. \tag{40}$$

The switching on condition, $\xi_{\mathbf{k}}(t<0)=0$, can be taken into account by the $\omega+i0^+$ substitution regularizing the way the Fourier transform is defined for zero frequency. From Eq. (40) one obtains

$$\xi_{\mathbf{k}}(\omega) = -\frac{a(\omega)}{\sqrt{2}\omega(2\varepsilon-\omega)}\begin{pmatrix}\omega h^*h'/\varepsilon - h^*h' - h^{*\prime}h\\ -\omega h^{*\prime} + \varepsilon h^{*\prime} + h^{*2}h'/\varepsilon\end{pmatrix}. \tag{41}$$

In the same order the ac conductivity is an integral over the sum of the paramagnetic and the diamagnetic contributions given by

$$\frac{j_{\mathbf{k}}(\omega)}{a(\omega)} = 4\frac{(h^*h'-h^{*\prime}h)^2}{\varepsilon(2\varepsilon+\omega)(2\varepsilon-\omega)} - 2\frac{h^*h''+hh^{*\prime\prime}}{\varepsilon}. \tag{42}$$

Subtracting a full derivative (independent of frequency), one can rewrite this as

$$\frac{j_{\mathbf{k}}(\omega)}{a(\omega)} = \frac{(h^*h'-h^{*\prime}h)^2}{\varepsilon^3}\frac{\omega^2}{4\varepsilon^2-\omega^2}. \tag{43}$$

Real and imaginary parts, taking the $\omega+i0^+$ definition into account, are

$$\mathrm{Re}\,\sigma = \frac{4}{i\omega}\sum_{\mathbf{k}}\frac{(h^*h'-h^{*\prime}h)^2}{\varepsilon} \times \lim_{s\to0}\frac{4\varepsilon^2-\omega^2+s^2}{[(2\varepsilon+\omega)^2+s^2][(2\varepsilon-\omega)^2+s^2]} = \frac{1}{4},$$

$$\mathrm{Im}\,\sigma = \frac{4}{i\omega}\sum_{\mathbf{k}}\frac{(h^*h'-h^{*\prime}h)^2}{\varepsilon} \times \lim_{s\to0}\frac{2\omega s}{[(2\varepsilon+\omega)^2+s^2][(2\varepsilon-\omega)^2+s^2]} = 0. \tag{44}$$

Therefore ac and dc conductivity are equal, as was also shown in recent calculations.[25] This is consistent with both the Kubo formula derivations[14] and optical experiments.[15] Similar results were obtained in multiple-layered graphene.[25]

A similar calculation can be performed directly in the t space (similar to the dc case) and shows that after a short transient one obtains the σ_2 value for the ac conductivity independent of frequency.

IV. BEYOND LINEAR RESPONSE. WEYL FERMIONS, PARITY ANOMALY AND THE NIELSEN-NINOMIYA THEOREM

As will be discussed below, an electric field should not necessarily be very small in graphene experiments so that corrections to linear response are of interest. In addition it is important to determine at what ballistic time-scale perturbation theory breaks down. In this section we present a perturbative calculation of the leading nonlinear effect in both dc and ac, and discuss the ways to regularize the Weyl model "correctly" in order to calculate these corrections.

A. Ultrarelativistic fermions near Dirac points

The tight-binding model employed here has two Dirac points around which the spectrum becomes ultrarelativistic $\varepsilon=v_g|\Delta_{L,R}\mathbf{k}|$, $\Delta_{L,R}\mathbf{k}=\mathbf{k}-\mathbf{K}_{L,R}$, see Fig. 1. In our units the

graphene velocity is $v_g=\frac{\sqrt{3}}{2}$. The matrix element of the tight-binding Hamiltonian can be expanded around K_L as

$$h_{\mathbf{k}}^L = v_g \exp\left(-i\frac{\pi}{3}\right)(\Delta k_x + i\Delta k_y). \tag{45}$$

The Weyl field describing the "left-handed"[18,26] fermions ψ^L, namely, a field satisfying the relativistic Dirac equation with zero fermion mass

$$i\partial_t \psi_1^L = v_g(\partial_x + i\partial_y)\psi_2^L,$$

$$i\partial_t \psi_2^L = v_g(\partial_x - i\partial_y)\psi_1^L, \tag{46}$$

can be constructed by the unitary transformation

$$\psi_1 = \psi_1^L, \quad \psi_2 = e^{-i(\pi/3)}\psi_2^L. \tag{47}$$

The matrix element around the second Dirac point $\mathbf{K}_R$ is different,

$$h_{\mathbf{k}}^R = v_g(\Delta k_x - i\Delta k_y) \tag{48}$$

and the Weyl fermions are "right-handed" particles that obey

$$i\partial_t \psi_1^R = v_g(\partial_x - i\partial_y)\psi_2^R,$$

$$i\partial_t \psi_2^R = v_g(\partial_x + i\partial_y)\psi_1^R \tag{49}$$

without any unitary transformation required. They belong to a different representation of the 2+1 dimensional Lorentz group.[27]

This is not just a peculiarity of the model but a rather general feature[6] of massless fermions on a lattice.[18,28] It is well known that in order to get a massless spectrum of fermionic excitations with any ultraviolet cutoff (hexagonal lattice is an example), they come in multiple locations on the Brillouin zone (species "doubling"). In the Hamiltonian formulation the multiplicity is 2^D, where D is the dimensionality of space, $D=2$ in graphene. In addition, the graphene fermions are "staggered," meaning the spinor components "live" on different sublattices of the honeycomb lattice. This reduces the doubling to $2^{D-1}=2$. The doubling is intimately linked to the parity (discrete chiral symmetry).[18,27] The two Dirac points have opposite chirality so that there is no "parity anomaly."

It is sometimes claimed in condensed-matter literature that, at least while doing linear response, one can concentrate on the two neighborhoods of the Dirac points and neglect the rest of the Brillouin zone. Even more, often the calculation's result is just multiplied by the factor 2 (the valley degeneracy). Below we show that this is generally not an accurate description of what happens. This is not an academic question since the low-energy Weyl theory is simpler than the tight-binding model and will be used in the next section to extend the calculations into higher orders in the electric field. One therefore needs a proper ultraviolet regularization of the Weyl model. Similar regularization issues are well known in field theory whenever chiral anomaly is encountered. Roughly, a "correct" regularization should respect the chiral symmetry leading to important constraints on the number and charges of massless fermions. Otherwise the model is called "anomalous" and results of perturbative calculations become arbitrary. The most famous example is the requirement that in each generation of elementary particles (leptons and quarks) the sum of charges should be zero.[29]

We therefore discuss in some detail the cancellation of infrared divergencies and the correct application of the "ultrarelativistic" approximation to the tight-binding model.

B. Cancellation of ultraviolet divergencies and the approximate chiral symmetry

The ultrarelativistic approximation, Eq. (45), fails when applied to the first term in the expression for conductivity σ_{BZ} given in Eq. (31). At first glance the integral in Eq. (31) is dominated by the two Dirac points since the integrand diverges there, see Fig. 2. For the both (widely separated) regions of the Brillouin zone, K_L and K_R, it has the same asymptotic form

$$\frac{(hh^{*\prime} - h^* h')^2}{2\varepsilon^3} - \frac{hh^{*\prime\prime} + h^* h''}{\varepsilon} \approx -\sqrt{3}\frac{(\Delta k_x)^2}{|\Delta \mathbf{k}|^3}. \tag{50}$$

The integral over the neighborhood of each Dirac point converges in the "infrared" (here meaning $\mathbf{k}\to\mathbf{K}_{L,R}$) due to the Jacobian $|\Delta\mathbf{k}|$ but is linearly divergent in the "ultraviolet" and both have the same sign, see Fig. 2. Hence the integration cannot be extended to infinity and the size of the Brillouin zone serves as a natural ultraviolet cutoff.

It is important to note that there is no cancellation of the divergence between the Dirac points since both have the same sign. The divergencies are. however, canceled by the contributions from regions of the Brillouin zone between the Dirac points in which the ultrarelativistic approximation is not valid. Therefore in the "Ohmic" regime during ballistic times one is not allowed to neglect states far from the Dirac points and replacement by the Weyl equation is incorrect. Due to cancellation of the whole "divergent" term, Eq. (31), one can devise an appropriate regularization in the UV in which these contributions are cancelled and even generalize the procedure to higher orders in the electric field. We propose and use such a scheme below in Sec. IV C. Simple recipes such as the momentum cutoff regularization (circles in Fig. 1) or giving the fermions an infinitesimal mass,[6] commonly used, may lead to unphysical results. As a consequence more sophisticated regularizations such as the ζ-function regularization,[11] "dimensional regularization"[29] and "Pauli-Villars" were developed for continuous field theories such as the Weyl model. The tight-binding model is very similar in this respect to the "lattice Hamiltonian" regularizations of the field theory (Hamiltonian meant here with time kept continuous) and also satisfies the chiral invariance criterion.[18]

C. Nonlinear response in dc. Where does the linear response break down?

Since the current density is an odd function of the electric field, the leading nonlinear correction to it appears in the third order in the field. The calculation along the lines of Sec. III A is quite straightforward albeit tedious. One can use the Weyl model instead of the tight-binding model due to the

following reason. It is well known in field theory that generally chiral anomaly effects, including the ultraviolet divergencies discussed in Sec. III D, appear only in one-loop calculations.[29] We checked and found that indeed up to the third order the expression is finite in the ultraviolet. Within the dynamical approach it is natural to perform the calculations without Fourier transforming into the ω space.

Up to the third order the current density is

$$j(t) = \frac{\mathcal{E}}{4}\left[1 + \frac{3}{64}t^4\mathcal{E}^2 + O(\mathcal{E}^4)\right]. \tag{51}$$

The correction therefore is growing as a large power of the ballistic time. It becomes as large as the leading order for $t = 2^{3/2}3^{-1/4}\mathcal{E}^{-1/2}t_\gamma$. Hence the perturbation theory breaks down on the time scale of

$$t_{nl} = \mathcal{E}^{-1/2}t_\gamma. \tag{52}$$

As will be seen in Sec. V, this agrees well with the crossover time obtained from a nonperturbative calculation. Of course this time should be larger than any other possible relaxation time (due to impurities, phonons, etc.) present in the system. A similar expansion was obtained for the number of electron-hole pairs.[16]

The result is the same for the tight binding and the corresponding Weyl model. The only issue would be the first-order calculation within the Weyl scheme since it is divergent in the ultraviolet. In Weyl model we used the momentum cutoff that will be described in Sec. IV B.

D. ac response and the third harmonic generation

An analogous calculation for the ac field $E=\mathcal{E}\cos(\omega t)$ switched on at $t=0$ results in

$$j(t)/\mathcal{E} = -\frac{1}{8\omega^4}\mathcal{E}^2 + \mathrm{Re}\ \sigma\cos(\omega t) + \mathrm{Im}\ \sigma\sin(\omega t) + \sigma_{3\omega}\cos(3\omega t) + O(\mathcal{E}^4). \tag{53}$$

The first term is just the reflection of the initial conditions and is nonuniversal. In the limit $\omega\to 0$ one recovers the dc result. The corrected value of the real (dissipative) part of the ac conductivity is

$$\mathrm{Re}\ \sigma = \frac{1}{4}\left[1 + \left(\frac{63}{128\omega^4} - \frac{9}{64\omega^2}t^2\right)\mathcal{E}^2\right]. \tag{54}$$

One observes that the perturbation theory is inapplicable for

$$\omega^2 < \mathcal{E} \quad \text{and} \quad t > \omega/\mathcal{E}. \tag{55}$$

This is less restrictive compared to the dc condition, Eq. (52) for $\omega > \mathcal{E}^{1/2}t_\gamma^{-1}$.

The present formulas can be compared with the results of the dynamical calculation beyond linear response by Mishchenko[20] in which a phenomenological model of relaxation was employed. For the inverse relaxation time Γ, his nonperturbative result is

$$\mathrm{Re}\ \sigma = \frac{\omega^2\Gamma^2}{2v_g^2\mathcal{E}^2}\left[\left(1 + \frac{v_g^2\mathcal{E}^2}{\omega^2\Gamma^2}\right)^{1/2} - 1\right] \approx \frac{1}{4}\left[1 - \frac{3\mathcal{E}^2}{16\omega^2\Gamma^2} + O(\mathcal{E}^4)\right].$$

This is consistent with the second correction terms in Eq. (54).

The inductive part was absent in linear response and now appears

$$\mathrm{Im}\ \sigma = \frac{3^3}{2^8\omega^3}t\mathcal{E}^2. \tag{56}$$

Due to the two conditions, Eq. (55), it is much smaller than σ_2. The third harmonic is generated with the real part

$$\sigma_{3\omega} = \frac{1}{2^9\omega^4}\mathcal{E}^2$$

while the inductive part is absent at the present order.

V. EXACT SOLUTION OF THE FIRST-QUANTIZED TIGHT-BINDING EQUATIONS

A. Application of the Floquet theory and reduction to one dimensional

It is a peculiar property of the tight-binding matrix Eq. (4) that the solution for arbitrary k_y can be reduced to that for $k_y=0$. Shifting the time variable to $\bar{t}=t-k_y/\mathcal{E}$, one can define an "universal wave function"

$$\bar{\psi}(\bar{t}) = \psi(t). \tag{57}$$

The Schroedinger Eq. (14) is now void of any k_y dependence,

$$i\partial_{\bar{t}}\bar{\psi}_1 = -(e^{-2i\Omega\bar{t}} + be^{i\Omega\bar{t}})\bar{\psi}_2,$$

$$i\partial_{\bar{t}}\bar{\psi}_2 = -(e^{2i\Omega\bar{t}} + be^{-i\Omega\bar{t}})\bar{\psi}_1, \tag{58}$$

where the dimensionless frequency $\Omega \equiv \mathcal{E}/(2\sqrt{3})$ is in units of t_γ^{-1}. The k_y component of the momentum enters the solution via the initial conditions Eq. (10) only. In terms of the universal function it takes the form

$$\psi_{\mathbf{k}}(t=0) = \bar{\psi}(\bar{t} = -k_y/\mathcal{E}) = u_{\mathbf{k}}. \tag{59}$$

Taking the Fourier transform of Eq. (58), the equations in frequency space turn into recursion relations

$$\omega\bar{\psi}_1(\omega) = -\bar{\psi}_2(\omega - 2\Omega) - b\bar{\psi}_2(\omega + \Omega), \tag{60}$$

$$\omega\bar{\psi}_2(\omega) = -\bar{\psi}_1(\omega + 2\Omega) - b\bar{\psi}_1(\omega - \Omega). \tag{61}$$

Floquet theory (and the recursion relations) assure that the frequencies are discrete and form two series both indexed by an integer m

$$\omega_m = \nu + 3\Omega m. \tag{62}$$

The "central" frequency ν will take generally two incommensurate values. Writing the Fourier amplitude $\bar{\psi}_1(\omega_m)$ as

p_m, one obtains, combining the two equations, Eqs. (60) and (61), the forward and the backward recursions,

$$p_m = \frac{\omega_m - 2\Omega}{b}\left[\omega_m - 3\Omega - \frac{1}{\omega_m - 5\Omega} - \frac{b^2}{\omega_m - 2\Omega}\right]p_{m-1} - \frac{\omega_m - 2\Omega}{\omega_m - 5\Omega}p_{m-2}, \tag{63}$$

$$p_m = \frac{\omega_m + \Omega}{b}\left[\omega_m + 3\Omega - \frac{1}{\omega_m + \Omega} - \frac{b^2}{\omega + 4\Omega}\right]p_{m+1} - \frac{\omega_m + \Omega}{\omega_m + 4\Omega}p_{m+2} \tag{64}$$

with normalization $p_0=1$. The p_1 and ν have to be determined by the consistency between the forward and the backward equations.

Generally there are two independent Floquet frequencies, however, our system is special with the exact relation

$$\nu^+ + \nu^- = 2\Omega, \tag{65}$$

which can be proven rigorously. This greatly simplifies the solution. To obtain a simple approximation, we expand around the easily solvable case of $k_x=\pi$ corresponding to $b=0$. In this case the solution consists of two frequencies

$$\nu^{\pm(0)} = \Omega \pm \sqrt{1+\Omega^2}, \tag{66}$$

where the superscript $^{(0)}$ denotes zeroth order in b. For experimentally accessible cases $\Omega \ll 1$, the Floquet frequencies are close to ± 1. We expand the Fourier coefficients in powers of b

$$p_m = p_m^{(0)} + bp_m^{(1)} + b^2 p_m^{(2)}, \tag{67}$$

where we do not distinguish for the time being between the two Floquet branches. Let us look for a solution with the initial choice

$$p_m^{(0)} = p^{(0)}\delta_m \tag{68}$$

which in particular means that $p_1=0$ at this order. It can be shown that the central frequency ν^+ does not have a first-order correction in b. Using this fact the forward recursion can be rewritten as

$$(\omega_m + \Omega)(\omega_m^2 - 2\Omega\omega_m - 1)p_m = b[(\omega_m + \Omega)p_{m-1} + (\omega_m - 2\Omega)p_{m+1}] + b^2(\omega_m - 2\Omega)p_m. \tag{69}$$

Inserting the expansions for p_m and ν into this relation yields the expression for $\nu^{+(2)}$,

$$\nu^{+(2)} = \frac{\nu^{(0)}/2 - \Omega}{\nu^{(0)2} - \Omega^2} - \frac{\nu^{(0)} - 5\Omega}{6\Omega(\nu^{(0)} - \Omega)(\nu^{(0)} - 2\Omega)(2\nu^{(0)} - 5\Omega)} + \frac{\nu^{(0)} - 2\Omega}{6\Omega(2\nu^{(0)} + \Omega)(\nu^{(0)2} - \Omega^2)} \tag{70}$$

so that the positive Floquet frequency (up to second order) is $\nu^+ = \nu^{(0)} + b^2\nu^{(2)}$. Moreover, it turns out that the expansion in b converges in the whole relevant range, $0 < b \leq 2$, and greatly assists the numerical solution of the recursion relation.

After the coefficients $p_m^{\pm}$ and Floquet frequencies $\nu^{\pm}$ are found, the solution of Eq. (58) is written in terms of the Fourier series

$$\bar{\psi}_{\mathbf{k}}^1(\bar{t}) = \sum_{s=\pm} A^s \sum_{m=-\infty}^{\infty} p_m^s e^{-i\omega_m^s \bar{t}},$$

$$\bar{\psi}_{\mathbf{k}}^2(\bar{t}) = \sum_{s=\pm} A^s \sum_{m=-\infty}^{\infty} \frac{p_m^s + bp_{m-1}^s}{\omega_m^{-s}} e^{i\omega_m^{-s}\bar{t}}. \tag{71}$$

The second line follows from Eq. (61), ω_m^s are defined in Eqs. (62) and (70) and we utilized Eq. (65) for simplification. The two complex coefficients A^s are fixed by the initial conditions Eq. (59). This solution is used to calculate the evolution of the current density, the energy, and the number of electron-hole pairs.

B. Results. Nonlinear regime and Bloch oscillations

The current density divided by the electric field (in physical units), $\sigma(t) \equiv J_y(t)/E$, is shown in Fig. 3 in Ref. 16 for various values of the dimensionless electric field $\mathcal{E}=E/E_0$. The (microscopic) unit of the electric field is very large $E_0 = \frac{\gamma}{ea} = 10^{10}$ V/m so that at realistic fields $\mathcal{E} \ll 1$. After an initial fast increase on the microscopic time scale t_γ, $\sigma(t)$ approaches the universal value $\sigma_2 = \frac{\pi}{2}\frac{e^2}{h}$ and settles there, consistent with the linear response, calculated in Sec. III B. Beyond the crossover time t_{nl} the conductivity rises linearly above the constant "universal" value σ_2

$$\frac{J(t)}{E} = \sigma_2 \lambda \mathcal{E}^{1/2}\frac{t}{t_\gamma}, \tag{72}$$

where $\lambda = 2^{5/2}3^{1/4}\pi^{-2} \simeq 0.75$. This is consistent with the Landau-Zener calculation (instantons) within the Weyl model,[17,30–32] see below. The crossover time, defined by $J(t_{nl})/E = \sigma_2$, is therefore

$$t_{nl} = \lambda^{-1}\mathcal{E}^{-1/2}t_\gamma \tag{73}$$

and is consistent with the perturbation theory breakdown ballistic time, Eq. (52). This linear increase regime can be considered as a precursor of the Bloch oscillations but is still universal in the sense that it depends solely on neighborhood of the Dirac points.

The current on the time scale of order

$$t_B = \frac{8\pi}{\sqrt{3}}\mathcal{E}^{-1}t_\gamma = 4\pi\frac{\gamma}{eEv_g} \tag{74}$$

exhibits Bloch oscillations, as is seen in Fig. 4 of Ref. 16, where larger fields in the range $\mathcal{E}=2^{-8}-2^{-5}$ are shown. It turns out that the current vanishes at points given *exactly* at multiples of $t_B/2$ with t_B being the period of the Bloch oscillations. One observes a peculiar feature that (apart from the relativistic initial constant segment) the time dependence of $\sigma(t)$ is similar for different electric fields. Indeed, if one plots $J/\sqrt{E}$ versus tE, all the curves nearly coincide. More-

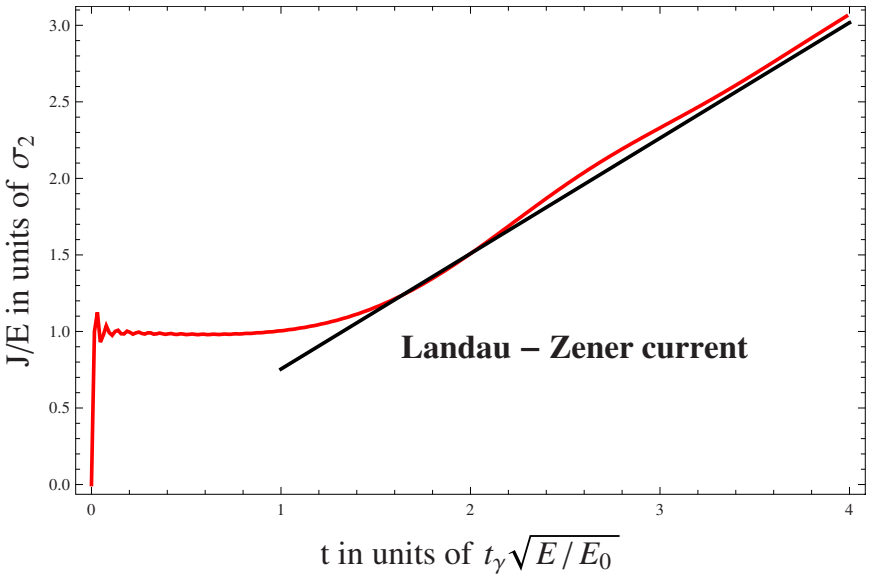

FIG. 4. (Color online) The time evolution of the dc conductivity in units of σ_2. The time is scaled with $\mathcal{E}^{-1/2}$ The simulations were performed in the field range $\mathcal{E}=2^{-12}-2^{-9}$ with UV cutoff equal to $1/a$. The straight line is the asymptotic linear behavior given by Eq. (72).

over, one obtains the following excellent fit for the current:

$$\frac{J(t)}{E} = \sqrt{3}\sigma_2 \mathcal{E}^{-1/2} \sin\left(\frac{\sqrt{3}t}{4t_\gamma}\mathcal{E}\right). \tag{75}$$

The Bloch time is approximately the time required for the electric field to shift the momentum across the Brillouin zone $\Delta p_y = eEt_B \sim \hbar/a$. This time scale is very long for experimentally achieved fields, much longer than the ballistic flight time. For example, in a sample of submicron length, $L=0.5$ μm, $t_{bal} \simeq 2.3\times 10^3 t_\gamma$. If one assumes that the electric current can reach $I_{\max}=1$ mA so for a typical width $W=1.5$ μm one has an electric field $E_{\max}=\frac{I_{\max}}{W\sigma_2}=10^7$ V/m corresponding to $\mathcal{E}=10^{-3}$ (the voltage in such case would be quite large $V_{\max}=E_{\max}L=5$ V). The first maximum of the Bloch oscillation will be seen at flight time of $t_B/4=3.6\times 10^3 t_\gamma$, which is of the same order as t_{bal}. If one uses a value of the current typical to transport measurements $I=50$ μA, the electric field is just $E=5\times 10^5$ V/m corresponding $\mathcal{E}=5\times 10^{-5}$ (voltage $V=250$ mV), $t_B/4=7.2\times 10^4 t_\gamma \gg t_{bal}$ and is therefore out of reach. See, however, a recent proposal.[33]

C. Crossover at t_{nl} in the Weyl model

It is expected that the transition to the nonlinear regime is dominated by the neighborhoods of the Dirac points. Therefore it can be obtained also within the Weyl model provided it is properly regularized in the ultraviolet region consistent with chiral symmetry, as was discussed in Sec. IV. For the calculation of the current density it suffices to renormalize the electric current by subtracting the UV divergent term Eq. (50)

$$J_y = -\frac{4v_g}{(2\pi)^2}\int_{|\mathbf{k}|<\Lambda}\left[\frac{1}{2}(\psi_2^*\psi_1+\psi_1^*\psi_2)+\frac{k_x^2}{|\mathbf{k}|^3}t\mathcal{E}\right]. \tag{76}$$

The results are practically indistinguishable compared to the tight-binding model for times larger than a microscopic time scale t_γ and much smaller than the Bloch time. Some examples of the tight-binding model were presented in Fig. 3 of Ref. 16. In Fig. 4 the conductivity in units of σ_2 is given as a function of time scaled with $\mathcal{E}^{-1/2}$. The function is the same for all electric fields as can be seen from scaling properties of the Weyl equations. The simulations were performed in the field range $\mathcal{E}=2^{-12}-2^{-9}$ with UV cutoff equal to $1/a$. The straight line is the asymptotic linear behavior given by Eq. (72). The asymptotic form is attained soon after t_{nl} so it looks like quite a sharp crossover.

Therefore this model can be effectively used to study the transition to the rapid creation of the electron-hole pairs and the creation of the electron-hole plasma but naturally cannot be used to see the transition to the Bloch oscillation regime.

Below we discuss the nature of the crossover to the nonlinear behavior and possible unique physics of the electron-hole plasma which might emerge.

VI. PHYSICAL PICTURE OF THE CROSSOVER TO THE NONLINEAR RESPONSE

A. Where does the energy go?

Beyond linear response one does not expect the current density to hold up to its linear-response value indefinitely. The situation differs from that in diffusive systems in which energy dissipates into heat due to inelastic scattering off impurities and phonons. In this case the system is not an isolated one but becomes part of a larger system including a "background." In an isolated ballistic system in a constant electric field the energy initially increases, as follows from the following argument. The total energy, Eq. (12), of electrons can be written in the first-quantized formalism as

$$U(t) = 2\langle\psi(t)|H|\psi(t)\rangle. \tag{77}$$

It can be shown using Eq. (9), that the power in this driven system is proportional to the current density

$$\frac{d}{dt}U = 2\langle\psi|\frac{d}{dt}H|\psi\rangle = -2eE\langle\psi|\frac{\partial H_{\mathbf{p}}}{\partial p_y}|\psi\rangle = EJ_y(t) \tag{78}$$

such as in dissipative systems. Consistently, as was shown above, the ballistic system has a finite conductivity such as a

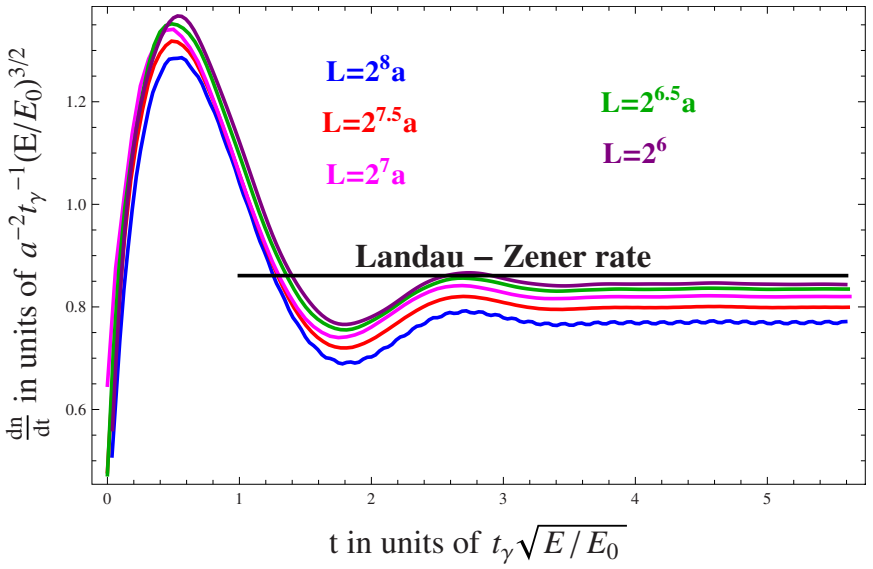

FIG. 5. (Color online) The electron-hole pair-creation rate as a function of time in units of $\mathcal{E}^{-1/2}t_\gamma$ for field $\mathcal{E}=2^{-10}$. The rate is scaled with $\mathcal{E}^{3/2}$. The ultraviolet cutoff is always $1/a$ while different curves represent different values for the infrared cutoff L/a.

dissipative system. We will refer to this as to quasi-Ohmic behavior.

Since the model does not provide a channel of dissipation, where does this "Joule-type" heat σE^2 go? The dynamical approach allows us to calculate the evolution of energy going beyond linear response. The energy of the system (calculated in a way similar to the current) is increasing continuously if no channel for dissipation is included. Therefore the conductivity originates in creation of pairs near the Dirac points with an additional contribution due to the turning of particles toward the field's direction. To gain more insight into the nature of the crossover to nonlinear response we also calculated the evolution of number of the electron-hole pairs during the ballistic flight.

B. Schwinger's pair-creation formula and graphene

The electron-hole creation rate by the dc electric field, $\frac{d}{dt}N_p$, with renormalized N_p defined in Eq. (38), is shown in Fig. 5 as a function of time for field $\mathcal{E}=2^{-10}$. Such a field $E=2^{-10}E_0=10^7$ V/m is quite realistic.[34,35] The rate is scaled with $\mathcal{E}^{3/2}$ while the time is given in units of $\mathcal{E}^{-1/2}t_\gamma$. The ultraviolet cutoff is always $1/a$, while different curves represent the infrared cutoff L/a. The length to width aspect ratio, L/W, is taken to be 1. The results do not depend significantly on it for all values presented, as long as $1/4 < L/W < 4$.

The time dependence of the rate exhibits the same time scales as the current density. At times smaller than t_{nl} the perturbative formula, Eq. (36) is valid. Immediately after switching on the electric field (times of order t_γ) the rate behaves as t^3. For $t_\gamma < t < t_{nl}$ the pair-creation rate per unit area rises linearly (with logarithmic corrections) according to Eq. (37). However, it is clear from Fig. 5 that the expansion breaks down at t_{nl} when the rate stabilizes, approaching the value (in our units of $a^{-2}t_\gamma^{-1}$)

$$\frac{d}{dt}N_p = \frac{8}{\pi^2 v_g^{1/2}}\mathcal{E}^{3/2}. \tag{79}$$

The power dependence of the rate on electric field, $E^{3/2}$ is the same as the rate of the vacuum breakdown due to the pair production calculated beyond perturbation theory by Schwinger in the context of particle physics (when generalized to the 2+1 dimensions and zero fermion mass[21,22]). It is not surprising since the power 3/2 is dictated by the dimensionality, assuming the ultrarelativistic approximation is valid. However, the physical meaning is somewhat different.

Note that the definition of the (renormalized) particle number, see Eq. (38), is different from the classical Schwinger's path-integral definition (which actually determines the "vacuum decay" rate rater than the pair-creation rate). The two are not the same within the Weyl model, as was shown asymptotically in the limit of large times in Ref. 24 and we obtain their value. The calculation of the number of pairs can be approximately performed using the instanton approach initiated by Nussinov in the context of particle physics[24] and extended in Refs. 17, 22, and 31. In condensed-matter physics the method is known as the Landau-Zener probability.[30,36] It provides an intuitive picture of Schwinger's pair-creation rate. Unfortunately this picture cannot be extended to ballistic times smaller than t_{nl} in which one cannot use the asymptotic large time expressions.

Note that in the Boltzmann equation approach to ballistic transport developed in Ref. 23 the renormalized pair number was utilized. This is connected to a simple relation within the Weyl model between the rate and the current density, as was shown recently.[30]

VII. DISCUSSION, CONCLUSIONS, AND GENERALIZATIONS

To summarize, we studied the dynamics of the electron-hole pair creation by an electric field in a single graphene sheet where the chemical potential is located right between the valence and the conduction bands. We assumed that the transport is purely ballistic, thus neglecting impurities, interaction with phonons, ripplons, as well as the screened interaction between electrons. The dynamical approach which

originated in particle physics[17] was adapted to the tight-binding model of graphene and allowed us to calculate the evolution of the current-density, energy and number of pairs beyond linear response. We clarified several delicate issues within linear response such as the correct dc conductivity value and a proper use of the ultrarelativistic Weyl model approximation to the tight-binding model. The question of proper regularization within the Weyl approximation was linked to the chiral (parity) symmetry and the anomaly cancellation in the tight-binding model. Using proper regularization the leading correction to the linear response in both dc and ac fields was calculated. The ac response which is purely pseudodissipative (no inductive part) and frequency independent in linear response shows strong frequency dependence, third harmonic generation and the inductive behavior.

It should be emphasized that beyond linear response new scales appear. Generally the tight-binding model in electric field has a time scale $t_\gamma=\hbar/\gamma$ *and* a dimensionless parameter $\mathcal{E}=E/E_0$ and $E_0=\gamma/(ea)$. In linear response the dimensionless parameter $\mathcal{E}$ does not appear in conductivity. This explains why the ac conductivity is independent of frequency all the way from optical frequencies $1/t_\gamma$ down to dc. Therefore it is not surprising that the dc conductivity is σ_2 rather than σ_1, which was obtained in numerous calculations over the years.[6,7,9,10] Some papers, in which both values are obtained in different limits,[8] even raise the question, what quantity is actually measured in experiments in "bulk" graphene such as those in Refs. 2 and 3? Within the dynamical approach there is no room for ambiguity since no regularizations, limits or uncontrollable approximations were used. We considered also finite-size effects for periodic boundary conditions and found that the conductivity converges to σ_2 for sizes of order $W,L\sim 50a$. We claim therefore that dc conductivity in graphene is a well defined physically measurable bulk quantity for a sufficiently large sample, $W,L\gg a$, and cannot have two different values within the same model. In particular, there is no dependence on the aspect ratio W/L for large samples contrary to the result of the Landauer approach. Therefore it is important to ask what could go wrong in other approaches to the same quantity in the same model.

The various approaches leading to this incorrect value σ_1 can be broadly divided into two classes. One type of calculations involves as the first step the introduction of disorder as a way to regularize the problem. At a later stage the disorder strength is taken to zero.[7,13] The calculation generally involves an uncontrollable resummation of diagrams. In addition to the Lindhart diagram, other diagrams (infinite series) involving disorder are summed. For a "regular" system this leads to the Drude formula with the correct limit (infinite conductivity) when the limit of vanishing disorder is taken. In graphene the nature of conductivity is different. There are no charge carriers and the electric field first has to create the carriers (electron-hole pairs) and only then to accelerate them. The acceleration is also quite specific: the absolute value of velocity is fixed while only the angle can change. The diagrams omitted in this process might not be small. There is no small parameter such as the Ioffe-Regel $\hbar/\varepsilon_F\tau$, where τ is the relaxation time, as in the regular case. One argues that due to "large" ε_F the other diagrams involving crossings are small. At the Dirac point $\varepsilon_F=0$ and this argument should be questioned. Therefore the use of the simplest resummation might be the origin of the error.

The second independent approach giving the same value σ_1 originates in mesoscopic physics. Disorder does not appear here and the only input is the description of "leads" and the boundary effects of the sample. Within the Landauer approach[10] one counts the "evanescent" modes in a ribbon of finite width W and length L leading to a result (for the armchair boundary conditions)

$$\sigma = 4\frac{e^2}{h}\frac{L}{W}\sum_{n=0}\cosh^{-2}(\pi n W/L) \underset{W/L\to\infty}{\to} \sigma_1. \tag{80}$$

It was claimed that the predictions including the finite sample conductivity and the Fano factor were confirmed by experiments[37] for very short samples on substrate. Note that the expression, Eq. (80), depends on the aspect ratio only, even when both W and L are large. We have performed calculations for finite samples with periodic boundary conditions (limited to $1/4<W/L<4$) and the results have a consistent large size limit of σ_2 irrespective of the aspect ratio. Thus there is a discrepancy between the two methods which should be further clarified.

Beyond the linear response the dimensionless parameter $\mathcal{E}$, in principle, can give rise to "macroscopic" time scales $t=\mathcal{E}^\alpha t_\gamma$. A rather unexpected result is that at a scale,

$$t_{nl} \simeq \frac{t_\gamma}{\sqrt{\mathcal{E}}} \simeq \sqrt{\frac{\hbar}{eEv_g}} \tag{81}$$

the physical behavior qualitatively changes. This time scale becomes the same as the ballistic time $t_{bal}=L/v_g=2\times 10^3 t_\gamma$ for length $L=0.5$ μm for relatively weak fields $\mathcal{E}=10^{-6}$ corresponding to $E=10^4$ V/m. It is important to note that this is the only time scale that enters the Weyl model approximation to the tight binding. Within this model the microscopic scale t_γ does not appear and t_{nl} is the only combination of the available parameters v_g and E. One could anticipate that the same scale appears in Weyl model as well.[30] Larger scales, however, can be formed in the tight-binding model. For example, at a scale $t_B=t_\gamma/\mathcal{E}$ Bloch oscillations set in. This is already beyond the Weyl approximation.

We therefore summarize the behavior of the conductivity and the number of electron-hole pairs in the various regimes at finite electric field E in turn.

Ballistic times $t<t_{nl}$. *Pseudodissipative behavior.* After a brief transient period (of order of several $t_\gamma=\hbar/\gamma$) the current density of the tight-binding model approaches a finite value and stabilizes there. Therefore the minimal dc electric conductivity at zero temperature is $\sigma_2=\frac{\pi}{2}\frac{e^2}{h}$. The pairs are created with various orientations of velocity (the value of which is fixed at v_g) and part of the current (the polarization or "zitterbewegung" part) is due to reorientation of the charge carriers. In this regime the pair-creation rate given by Eq. (37) is small enough so that pairs can be considered independent, provided the number density of created pairs $\frac{e^2E^2\gamma}{\hbar^2}t^2$ is not too large. If it is very large the inverse process of pair annihilation (via various channels) cannot be neglected. Ap-

proaching t_{nl} the perturbation theory breaks down. At this time the density of pairs is $\frac{eE}{a}$. It becomes on the order of 10^{11} cm^{-1} for $E=10^5$ V/m. Let us assume that this does not happen and proceed to the longer ballistic times.

Ballistic times $t_{nl}<t<t_B$. Schwinger's pair creation and formation of the electron-hole plasma. On the larger time scale nonperturbative methods should be used. The pair creation is more intensive and the pair density asymptotically follows an analog of the Schwinger's formula for massless fermions in 2+1 dimensions, Eq. (14). The current above t_{nl} increases linearly with time

$$J(t)=\sigma_2\left(\frac{\sqrt{3}}{2}E\right)^{3/2}\left(\frac{ev_g}{\hbar}\right)^{1/2}t. \tag{82}$$

In this regime most of the electrons are oriented along the field direction so that $J=2ev_gN(t)$. For example, in order to reach the density of $N=10^{11}$ cm^{-2} in a sample with ballistic time $t_b=L/v_g=2000t_\gamma(L=0.5\ \mu\text{m})$ the field should reach $E=10^4$ V/m. If the sample is short enough the transport still can be ballistic but due to its nonlinear nature a more likely scenario is that a dissipation channel opens up.

One can only speculate what kind of dissipation process truncates the pair creation and stabilizes the electron-hole plasma created by the electric field. Of course, the standard candidates are collisions with impurities, phonons, ripplons, and the electron-electron interactions. Here we point out that the system is "open" and one should consider the "radiation friction" scenario: pairs annihilate emitting photons which take energy out of the graphene sheet. The effects of radiation of energy into space might in principle be observable at elevated fields and should be investigated.

Ballistic times $t>t_B$. Bloch oscillations. If the system is still ballistic at yet longer times, Bloch oscillations set in with a period of $t_B=\frac{\hbar}{eaE}=t_\gamma/\mathcal{E}$. This time scale becomes the same as the ballistic time $t_{bal}=2\times10^3t_\gamma$ for relatively weak fields $\mathcal{E}=10^{-3}$ corresponding to $E=10^7$ V/m, see Fig. 2 in Ref. 16. While the Bloch oscillations are difficult to observe (see, however, a recent proposal[33]), the transition to a nonlinear regime is within reach of current experimental techniques.

The dynamic approach was generalized to bilayer graphene[38] in which similar questions exist for a long time. The correct dc conductivity for the N layered graphene is equal to the dynamical one $\sigma=N\sigma_2$, consistent with the vanishing frequency limit of the ac conductivity.[25] The creation of the electron-hole plasma is even more likely in these systems.

In this paper only ballistic transport was considered. In principle, disorder and electron-electron interactions could be incorporated within the dynamical approach in the way the Boltzmann equation approach[23,39] can be extended beyond the linear response. In fact, using a phenomenological methodology, disorder has recently been incorporated for the ac field in Ref. 20. Similarly Coulomb interactions and the pair annihilations into photons, phonons, etc., can be taken into account. Generally though, when the system has a large number of electron-hole pairs, the screening by the neutral plasma is more effective and the influence of impurities and interactions diminishes. Understanding these effects is crucial for investigating the (nonlinear) plasma waves and their damping.[40]

Let us note the relation between the dynamics on the time scale t_{nl} and quantum adiabatic transport near the quantum critical point.[36,41] The calculation of the number of pairs can be approximately performed using the instanton approach initiated in the context of particle physics[24] and extended in Refs. 17, 22, and 31. In condensed-matter physics the method is known as the Landau-Zener probability.[30,36] It provides an intuitive picture of the Schwinger's pair-creation rate. The ballistic evolution in graphene therefore can be considered as an example of the adiabatic quantum evolution which attracted much attention recently in connection to the Kibble-Zurel mechanism of phase-transition dynamics and others. Graphene dynamics at large ballistic times offers an accessible system in which these processes can be observed.

Finally let us remark on the application of the dynamical approach to calculating the response to very short strong-field pulses such as the femtosecond (and an order of magnitude longer) laser pulses. A possibility of measuring the response to such fields was advocated by Rusin and Zawadzki.[42] For this purpose the dynamical linear-response formulas, as presented in the Sec. III, can be directly applied for arbitrary time dependence of the pulse while the nonlinear calculation of Sec. V describes the steplike pulse of finite duration only. Other shapes of the pulse can be calculated by breaking the pulse into several segments of different constant field.

ACKNOWLEDGMENTS

We are indebted to J. Santoro, E. Andrei, M. Deshmukh, A. F. Morpurgo, V. Singh, E. Farber, and W. B. Jian for valuable discussions. Work of B.R. and H.K. was supported by NSC of R.O.C. under Grants No. 98-2112-M-009-014-MY3 and No. 98-2112-M-003-002-MY3, respectively, the National Center for Theoretical Sciences, and MOE ATU program. B.R. acknowledges the hospitality of the Applied Physics Department of AUCS; M.L. acknowledges the hospitality and support of the NCTS.

*vortexbar@yahoo.com

[1] S. V. Morozov, K. S. Novoselov, M. I. Katsnelson, F. Schedin, D. Elias, J. A. Jaszczak, and A. K. Geim, Phys. Rev. Lett. **100**, 016602 (2008).

[2] X. Du, I. Skachko, A. Barker, and E. Y. Andrei, Nat. Nanotechnol. **3**, 491 (2008).

[3] K. I. Bolotin, K. J. Sikes, J. Hone, H. L. Stormer, and P. Kim, Phys. Rev. Lett. **101**, 096802 (2008).

[4] M. Lewkowicz and B. Rosenstein, Phys. Rev. Lett. **102**, 106802 (2009).
[5] A. H. Castro Neto, F. Guinea, N. M. R. Peres, K. S. Novoselov, and A. K. Geim, Rev. Mod. Phys. **81**, 109 (2009); V. P. Gusynin, S. G. Sharapov, and J. P. Carbotte, Int. J. Mod. Phys. B **21**, 4611 (2007).
[6] V. P. Gusynin and S. G. Sharapov, Phys. Rev. B **73**, 245411 (2006).
[7] T. Ando, Y. Cheng, and H. Suzuura, J. Phys. Soc. Jpn. **71**, 1318 (2002); N. M. R. Peres, F. Guinea, and A. H. Castro Neto, Phys. Rev. B **73**, 125411 (2006).
[8] A. W. W. Ludwig, M. P. A. Fisher, R. Shankar, and G. Grinstein, Phys. Rev. B **50**, 7526 (1994); K. Ziegler, Phys. Rev. Lett. **97**, 266802 (2006); Phys. Rev. B **75**, 233407 (2007); S. Ryu, C. Mudry, A. Furusaki, and A. W. W. Ludwig, *ibid.* **75**, 205344 (2007); J. Cserti, *ibid.* **75**, 033405 (2007).
[9] M. I. Katsnelson, Eur. Phys. J. B **51**, 157 (2006).
[10] J. Tworzydlo, B. Trauzettel, M. Titov, A. Rycerz, and C. W. J. Beenakker, Phys. Rev. Lett. **96**, 246802 (2006); E. B. Sonin, Phys. Rev. B **79**, 195438 (2009).
[11] C. G. Beneventano, P. Giacconi, E. M. Santangelo, and R. Soldati, J. Phys. A **42**, 275401 (2009).
[12] K. S. Novoselov, A. K. Geim, S. V. Morozov, D. Jiang, M. I. Katsnelson, I. V. Grigorieva, S. V. Dubonos, and A. A. Firsov, Nature (London) **438**, 197 (2005); Y. Zhang, Y.-W. Tan, H. L. Stormer, and P. Kim, *ibid.* **438**, 201 (2005).
[13] E. Fradkin, Phys. Rev. B **33**, 3263 (1986).
[14] L. A. Falkovsky and A. A. Varlamov, Eur. Phys. J. B **56**, 281 (2007).
[15] R. R. Nair, P. Blake, A. N. Grigorenko, K. S. Novoselov, T. J. Booth, T. Stauber, N. M. R. Peres, and A. K. Geim, Science **320**, 1308 (2008).
[16] B. Rosenstein, M. Lewkowicz, H. C. Kao, and Y. Korniyenko, Phys. Rev. B **81**, 041416(R) (2010).
[17] E. S. Fradkin, D. M. Gitman, and S. M. Shvartsman, *Quantum Electrodynamics with Unstable Vacuum* (Springer-Verlag, Berlin, 1991); S. P. Gavrilov and D. M. Gitman, Phys. Rev. D **53**, 7162 (1996).
[18] L. Karsten and J. Smit, Nucl. Phys. B **183**, 103 (1981); J. Smit, *Introduction to Quantum Fields on a Lattice* (Cambridge Univesity Press, New York, 2002).
[19] S. A. Mikhailov, EPL **79**, 27002 (2007).
[20] E. G. Mishchenko, Phys. Rev. Lett. **103**, 246802 (2009).
[21] J. Schwinger, Phys. Rev. **82**, 664 (1951); G. Dunne and T. Hall, Phys. Rev. D **58**, 105022 (1998); S. P. Kim, H. K. Lee, and Y. Yoon, *ibid.* **78**, 105013 (2008).
[22] T. D. Cohen and D. A. McGady, Phys. Rev. D **78**, 036008 (2008).
[23] L. Fritz, J. Schmalian, M. Müller, and S. Sachdev, Phys. Rev. B **78**, 085416 (2008).
[24] A. Casher, H. Neuberger, and S. Nussinov, Phys. Rev. D **20**, 179 (1979); D. Allor, T. D. Cohen, and D. A. McGady, *ibid.* **78**, 096009 (2008).
[25] W. K. Tse and A. H. MacDonald, Phys. Rev. B **80**, 195418 (2009).
[26] S. Weinberg, *The Quantum Theory of Fields*, Modern Applications Vol. 2 (Cambridge University Press, Cambridge, England, (2005).
[27] A. Coste and M. Luscher, Nucl. Phys. B **323**, 631 (1989).
[28] H. B. Nielsen and M. Ninomiya, Nucl. Phys. B **185**, 20 (1981); **193**, 173 (1981).
[29] M. E. Peskin and D. V. Schroeder, *An Introduction to Quantum Field Theory* (Westview Press, Boulder, CO, 1995); L. H. Ryder, *Quantum Field Theory* (Cambridge University Press, Cambridge, England, 1996).
[30] B. Dóra and R. Moessner, Phys. Rev. B **81**, 165431 (2010).
[31] S. P. Kim and D. N. Page, Phys. Rev. D **65**, 105002 (2002).
[32] M. Koshino and T. Ando, Phys. Rev. B **73**, 245403 (2006); J. Cserti, A. Csordas, and G. David, Phys. Rev. Lett. **99**, 066802 (2007).
[33] D. Dragoman and M. Dragoman, Appl. Phys. Lett. **93**, 103105 (2008).
[34] V. Singh and M. M. Deshmukh, Phys. Rev. B **80**, 081404(R) (2009).
[35] I. Snyman and C. W. J. Beenakker, Phys. Rev. B **75**, 045322 (2007).
[36] F. Pellegrini, S. Montangero, G. E. Santoro, and R. Fazio, Phys. Rev. B **77**, 140404(R) (2008); D. Patanè, L. Amico, A. Silva, R. Fazio, and G. E. Santoro, *ibid.* **80**, 024302 (2009).
[37] F. Miao, S. Wijeratne, Y. Zhang, U. C. Coskun, W. Bao, and C. N. Lau, Science **317**, 1530 (2007); L. DiCarlo, J. R. Williams, Y. Zhang, D. T. McClure, and C. M. Marcus, Phys. Rev. Lett. **100**, 156801 (2008); R. Danneau, F. Wu, M. F. Craciun, S. Russo, M. Y. Tomi, J. Salmilehto, A. F. Morpurgo, and P. J. Hakonen, *ibid.* **100**, 196802 (2008).
[38] Y.-X. Wang, L.-P. Shi, and S.-J. Xiong, EPL **87**, 57002 (2009).
[39] M. Auslender and M. I. Katsnelson, Phys. Rev. B **76**, 235425 (2007); E. G. Mishchenko, Phys. Rev. Lett. **98**, 216801 (2007); R. Bistritzer and A. H. MacDonald, Phys. Rev. B **80**, 085109 (2009).
[40] A. Konar, T. Fang, and D. Jena, arXiv:0902.0819 (unpublished).
[41] S. Sachdev, *Quantum Phase Transitions* (Cambridge University Press, Cambridge, England, 2000).
[42] T. M. Rusin and W. Zawadzki, Phys. Rev. B **78**, 125419 (2008); **80**, 045416 (2009).